PCCP

View Online
Dynamic Article Links

Cite this: DOI: 10.1039/c0cp02409k

www.rsc.org/pccp

PAPER

Electrochemistry of $Os(2,2'\text{-bpy})_2ClPyCH_2NHCOPh$ tethered to Au electrodes by S–Au and C–Au junctions†

A. M. Ricci,[a] N. Tognalli,[b] E. de la Llave,[a] C. Vericat,[c] Lucila P. Méndez De Leo,[a] Federico J. Williams,[a] D. Scherlis,[a] R. Salvarezza[c] and E. J. Calvo*[a]

Received 5th November 2010, Accepted 10th February 2011
DOI: 10.1039/c0cp02409k

Osmium pyridine-bipyridine redox centers have been tethered to Au electrodes by chemical modification through Au–S and Au–C bonds respectively. 4-mercapto benzoic acid and the reduction product of the aryl diazonium salt of 4-amino benzoic acid were reacted on Au surfaces, with further post-functionalization by chemical reaction of the osmium complex amino-pyridine derivative with the surface carboxylates. The resulting modified Au surfaces were characterized by polarization modulated infrared reflection absorption spectroscopy (PM-IRRAS), scanning tunneling microscopy (STM), X-ray photoelectron spectroscopy (XPS), resonant raman spectroscopy and cyclic voltammetry.

Introduction

Electrode surface modification with organic molecules has been the subject of many studies because it can improve the properties of the material and lead to its application in electrocatalysis,[1] bioelectrocatalysis,[2] biosensors,[3] solar photoconversion[4] and molecular electronics,[5,6] among others. They can also be used as model systems to analyze the electron transfer rate by including redox groups in organized monolayers.[7–12]

The most popular method for the derivatization of coinage metal electrodes is thiol self-assembly, especially on gold. This technique yields well organized, compact monolayers which are easy to prepare and stable in a wide potential window. A wide variety of functional groups can be added to these molecules making it a very attractive strategy for chemically modifying surfaces.[13,14]

The reduction of diazonium salts has gained some prominence during recent years, and it is an alternative way to form thin layers on different materials. It was introduced by Pinson in 1992[15,16] and subsequently other authors contributed to its development.[17–20] This technique can be applied to different materials: different varieties of carbon,[21–24] semiconductors (silicon[25] and GaAs[26]), gold[27,28] and also Pt, Si, Fe, Cu, Co, Zn, Ni.[29–31] Therefore, this methodology constitutes a surface modification tool that can be applied in principle to all types of substrates. In this case, the electroreduction of a diazonium salt generates an aryl radical that can react with the electrode, forming a covalent bond with it. Therefore, it is an easy technique to implement that generates stronger links between the substrate and molecules than the one obtained by thiol self-assembly yielding films more difficult to desorb because of the strong metal–C covalent bond. Different techniques have been employed in their characterization: FT-IRRAS,[28,30,32] XPS,[27,30,31] AFM[23,30] and Raman Spectroscopy.[31,32]

The organic films attached to the surface by either strategy can be further post-functionalized using different chemical routes described in the literature. The reaction between grafted amino groups and acid anhydride,[33] click chemistry[34] or the coupling between amino groups and epoxy groups[24] are good examples of surface post-functionalization. One of the most widely used strategies is the carbodiimide chemistry.[35–40] In particular, either of these chemical reactions can be used to attach redox centers to the surface.[12,35,41–43]

In the present article we report on gold electrodes modified with the $Os(2,2'\text{-bpy})_2PyCH_2NHCOPhX$ complex, where X = C, S; *i.e.* the same redox molecule has been tethered to the surface through different anchoring atoms (X). Both systems have been characterized by polarization modulated infrared absorption-reflection spectroscopy (PM-IRRAS), resonant Raman spectroscopy, scanning tunneling microscopy (STM), X-ray photoelectron spectroscopy (XPS) and cyclic voltammetry. Finally, density functional theory (DFT) calculations were used to determine projected density of states

[a] *INQUIMAE, Facultad de Ciencias Exactas y Naturales, Universidad de Buenos Aires, CONICET Pabellón 2, Ciudad Universitaria, 1428 Buenos Aires, Argentina. E-mail: calvo@qi.fcen.uba.ar; Fax: 541145763341; Tel: 541145763378*
[b] *Centro Atómico Bariloche and Instituto Balseiro, Comisión Nacional de Energía Atómica, 8400 S. C. de Bariloche, Río Negro, Argentina*
[c] *INIFTA, Universidad Nacional de La Plata, CONICET, Sucursal 4 Casilla de Correo 16, 1900 La Plata, Argentina*
† This article is part of the special collection on interfacial processes and mechanisms in celebration of John Albery's 75th birthday.

(PDOS) of gold slabs modified with benzene and mercaptobenzene, respectively. This analysis provides an insight of the interactions governing the two types of bond: Au–C and Au–S.

Experimental

Chemicals

The following chemicals were used as received: 4-mercaptobenzoic acid (Sigma–Aldrich), tetrafluoroborate tetrabutylammonium (Fluka), 4-aminobezoic acid (Sigma–Aldrich), iso-amyle nitrite (Sigma–Aldrich), tetrafluoroboric acid (50% solution, Riedel de Haën), ethyl ether (Sintorgan), 1-ethyl-3-(3-dimethylamino-propyl)-carbodiimide (Aldrich), N-hydroxy-succinimide (Aldrich), 4-2-hydroxyethyl-1-piperazineethanesulfonic acid (HEPES) (Sigma–Aldrich), potassium nitrate (Merck), sodium nitrate (Biopack), ethanol, acetonitrile (Sintorgan).

Preparation of gold surfaces and modification with osmium complexes

Silicon (100) substrates were coated with a 20 nm titanium and 20 nm palladium adhesion layer and a 200 nm gold layer, thermally evaporated with an Edwards Auto 306 vacuum coating system at $P < 10^{-8}$ bar, and employed as electrodes. Surface contamination of the gold substrates employed as working electrodes was always controlled before its modification. For this purpose, cyclic voltammetry was performed in a solution of 2 M H_2SO_4, sweeping the potential between 0.1 and 1.6 V at 0.1 V s^{-1}. The electrochemically active area of the electrodes was also estimated from the charge of the gold oxide reduction peak: it was considered that the adsorption sites of small molecules, such as H_2 or O_2, are the same that participate in electrochemical reactions of interest. To calculate the effective area of electrode, the charge corresponding to the electrochemical desorption of a monolayer of oxygen (reduction peak of Au) of 400 μC cm^{-2} [44,45] was taken as reference. In general, the factor roughness found by this method for evaporated gold electrodes was 1.5–2. A glass electrochemical cell with a Pt counter electrode and an Ag/AgCl, 3 M KCl reference electrode was employed, and potentials herein are reported with respect to this reference. For STM measurements evaporated Au films on glass with (111) preferred orientation (AF 45 Berliner Glass KG, Germany) were used as substrates. After soft annealing with a hydrogen flame these Au substrates exhibit atomically smooth (111) terraces separated by monatomic steps in height.

The complex $[Os(bpy)_2Cl(py\text{-}CH_2\text{-}NH_2]PF_6$ was grafted to both types of gold electrodes by post-functionalization of 4-mercaptobenzoic and benzoic acid monolayers, respectively. In the first case, the gold surface was dipped in 1 mM 4-mercaptobenzoic acid solution in ethanol overnight, while the benzoic acid monolayer was obtained by electrochemical reduction of the corresponding diazonium salt using chronoamperometry (0.4 V, 5 min in 5 mM 4-carboxy-benzenediazonium tetrafluoroborate 0.1 M tetrabutylammonium tetrafluoroborate/acetonitrile). The synthesis of the osmium complex and the diazonium salt are described elsewhere.[43] After derivatization, the gold surfaces were incubated in 40 mM 1-ethyl-3-(3-dimethyl-amino-propyl)-carbodiimide (EDC)/10 mM N-hydroxysuccinimide (NHS) solution for 1 h, and dipped in 0.25 mM $[Os(bpy)_2Cl(py\text{-}CH_2\text{-}NH_2]PF_6$/0.05 M HEPES buffer (N-2-hydroxyethylpiperazine-N′-2-ethanesulfonic acid) pH 7.3, I = 0.1 M KNO_3 for 12 h.

IR experiment

Polarization modulation infrared reflection absorption spectroscopy (PM-IRRAS) experiments were performed on a Thermo Nicolet 8700 (Nicolet, Madison, WI) spectrometer equipped with a custom-made external table-top optical mount, a MCT-A detector (Nicolet), a photoelastic modulator, PEM (PM-90 with II/Zs50 ZnSe 50 kHz optical head, Hinds Instrument, Hillsboro, OR), and synchronous sampling demodulator, SSD, (GWC Instruments, Madison, WI). The IR spectra were acquired with the PEM set for a half wave retardation at 1450 cm^{-1} for the CH bending and aromatic region and for stretching modes associated with the COOH group. The angle of incidence was set at 80°, which gives the maximum of mean square electric field strength for the air/gold interface. The demodulation technique developed by Corn[46,47] was used in this work. The signal was corrected by the PEM response using a method described by Frey *et al.*[48] Typically 1000 scans were performed and the resolution was set for 4 cm^{-1}. Transmission spectrum for crystalline $[Os(2,2'\text{-}bpy)_2ClPyCH_2NH_2]PF_6$ was measured using a KBr pellet with 4 cm^{-1} resolution and performing 200 scans.

Raman experiment

The resonant Raman scattering experiments were performed using a Jobin–Yvon T64000 triple spectrometer operating in subtractive mode and equipped with a liquid N_2 cooled charge coupled device. The spectra were taken using 10 mW of both the 514.5 and the 530 nm lines of an Ar–Kr laser in air and in contact with the electrolyte as a function of the electrode potential. The acquisition time was 10 s and the potential was cycled between 100 and 600 mV *vs.* Ag/AgCl at a 10 mV s^{-1} scan rate. A line focus, ≈2 mm long and ≈100 μm wide was chosen to reduce the photon-induced degradation of the osmium complex (photobleaching by ligand exchange aquation).

XPS experiments

X-ray photoelectron spectroscopy measurements (XPS) were performed under UHV conditions (base pressure $<5.10^{-10}$ mbar) in a SPECS UHV spectrometer system equipped with a 150 mm mean radius hemispherical electron energy analyzer and a nine channeltron detector. XPS spectra were acquired at a constant pass energy of 20 eV using an non-monochromated MgKα (1253.6 eV) source operated at 12.5 kV and 20 mA and a detection angle of 30 degrees with respect to the sample normal on grounded conducting substrates. Quoted binding energies are referred to the Au 4f7/2 emission at 84 eV. Atomic ratios and surface concentrations were calculated from the integrated intensities of core levels after instrumental and photoionization cross-section corrections assuming linear backgrounds in all cases. In principle atomic

ratios have to be interpreted with great care since photoelectrons arising from atoms near the substrate are attenuated by the overlying material. Thus, the sulfur signal is attenuated due to inelastic scattering of the photoelectrons by the monolayer. The measured atomic composition is thus sensitive to the elemental distribution perpendicular to the surface in addition to the actual composition of the layer. However, we should also bear in mind that the adsorbate layer is far from being a dense monolayer and that the detection angle employed was not grazing, therefore measured atomic ratios would not deviate much from real atomic ratios.

STM measurements

Scanning tunneling microscopy (STM) imaging was performed in air in the constant current mode with a Nanoscope IIIa microscope from Veeco Instruments (Santa Barbara, CA) by using commercial Pt–Ir tips. Typical ranges for tunneling currents, bias voltages and scan rates were 0.3–3 nA, 1.0–1.5 V and 1–2 Hz, respectively.

Electrochemical experiment

Electrochemical measurements were carried out with an Autolab V 30 system (Eco Chemie, Utrecht, the Netherlands) controlled by a General Purpose Electrochemical Software (GPES) with 750 kHz bandwidth ADC750 fast sampling module and scangen analog sweep module. All experiments were carried out at room temperature (20 ± 2 °C) in a purpose-built, three-electrode Teflon cell, with an electrode exposed area of approximately 0.28 cm^2 limited by an inert "o" ring.

Density functional theory calculations

Plane-waves density functional calculations in periodic boundary conditions were performed with the Quantum Espresso code.[49] Ultrasoft type pseudo-potentials were adopted to represent the ion-electron interactions,[50] in combination with the PBE formalism to compute the exchange–correlation term.[51] An energy cutoff of 25 and 200 Ry was used for the plane-waves expansion of the Khon-Sham orbitals and the charge density, respectively. The Au(111) surface was modeled as an infinite bidimensional slab consisting of four layers of Au atoms, with 12 atoms per layer. Unit cell dimensions were set according to the DFT optimized lattice constant of the gold *fcc* structure (4.08 Å), and leaving a vacuum space of about 12 Å in between the slabs. The sampling of the Brillouin zone was done with a $3 \times 2 \times 1$ Monkhorst–Pack grid.[52]

Results and discussion

The structures of the $Os(2,2'\text{-bpy})_2ClPyCH_2NHCOPhX$ complexes grafted onto the gold surface are depicted in Scheme 1 for (a) the osmium complex attached by the sulfur atom obtained by the self-assembly of 4-mercaptobenzoic acid and its post-functionalization with $[Os(bpy)_2Cl(py\text{-}CH_2\text{-}NH_2]PF_6$ and (b) the complex attached to the aryl group on the surface, obtained after the electroreduction of the diazonium salt derived from *p*-amino benzoic acid (4-carboxybenzenediazonium tetrafluoroborate). Herein we shall refer to these systems as Au/ SPhCOOH/Os and Au/PhCOOH/Os, respectively.

Electrochemical experiment

The Os complex-modified gold electrodes were characterized by cyclic voltammetry in order to confirm the presence of the redox centers on the surface. Fig. 1 depicts the cyclic voltammograms obtained for both systems in 0.1 M $NaNO_3$ at 0.1 V s^{-1}. The formal potential ($E^{\circ\prime}$) was determined as the average of the anodic and cathodic peak positions. The complex surface coverage (Γ_{Os}) was estimated from the electrochemical charge involved in the oxidation-reduction of the redox couple, taking the ratio between the average area below the anodic and cathodic peaks and the scan rate. In these calculations, we considered the gold substrate surface areas obtained from the cyclic voltammetry in H_2SO_4 2M described above.

Finally, the full widths at half maximum (FWHM) were also obtained (see Table 1).

The voltammograms in Fig. 1 have the characteristic shape of an electroactive species tethered to the surface of an electrode. In both cases we observed a linear relationship between the peak current and the scan rate, indicating that a constant number of redox centers attached to the surface can be switched between reduced and oxidized states.[53]

Moreover, the anodic and cathodic charges are almost equal suggesting that the Os bipyridine complex can be completely oxidized and reduced under these conditions. The formal potential in both cases is $\approx$0.30 V and is in good agreement with the reported values for this and other similar complexes adsorbed on electrode surfaces.[9,10,35] Taking as a reference the formal potential in solution (0.24 V) of a soluble analogous ($[Os(2,2'\text{-bpy})_2ClPyCHO)]^+$),[54] we can appreciate that there is a positive shift of $E^{\circ\prime}$ when the redox couple is on the surface, which can be attributed to surface potential effects and charge regulation.

Since the osmium complex has a positive charge in both oxidation states, the oxidation process implies an increment of the electrostatic repulsions between neighboring molecules. This effect could explain why the formal potential shifts positively when the redox couple is confined to a surface.

Non ideal voltammetric surface waves in Fig. 1 are characterized by a peak separation $\Delta E_p > 0$ at low scan rates, and a full width at half maximum (FWHM) larger than the expected value of 90.6 mV for an ideal one-electron redox process. Both observations can be related to the repulsive interactions between positively charged redox centers.

The surface area occupied by a single molecule of the osmium complex was estimated by theoretical considerations based on the density functional theory (DFT). The theoretical structure of the molecule tethered to the surface was constructed by two DFT optimized fragments: the osmium complex and the benzoic acid (or the 4-mercaptobenzoic acid) attached to the gold surface. These two fragments were combined and partially relaxed to optimize the bond between them. This treatment led to an occupied surface area of 120 $Å^2$ per complex molecule. Therefore a surface coverage of 1.38×10^{-10} mol cm^{-2} (or 13.3 μC cm^{-2}) was estimated for a compact osmium complex monolayer. From this estimation, we conclude that the surface coverage obtained from the electrochemical analysis for both systems is very close to the theoretically expected value. Moreover, it is in very good

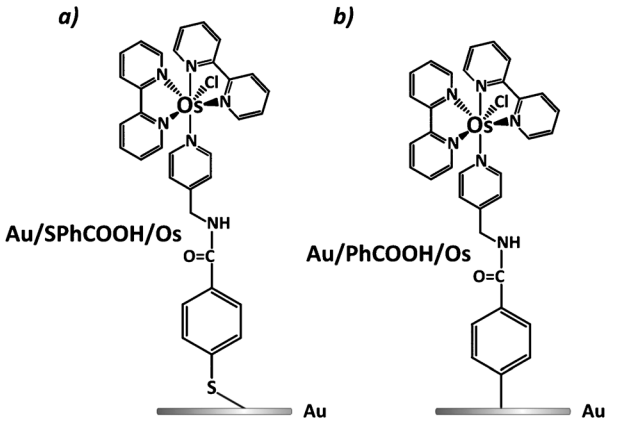

Scheme 1 Schematic structure of the redox couple Os(II)/Os(III) tethered to a gold surface by (a) a S–Au bond and (b) a C–Au bond. These systems were obtained by post-functionalization of a previous formed SAM of 4-mercaptobenzoic acid and a thin film resulting from the reduction of 4-carboxybenzenediazonium tetrafluoroborate, respectively, with the $[Os(2,2'\text{-bpy})_2ClPyCH_2NH_2]PF_6$ complex.

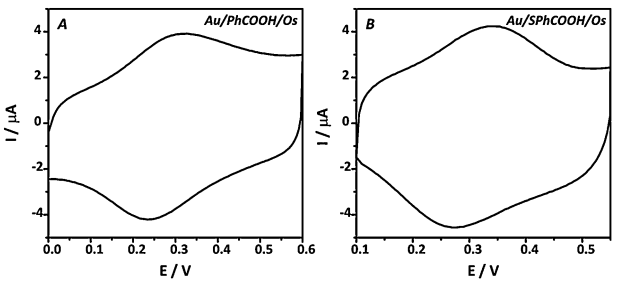

Fig. 1 Cyclic voltammetry of a gold electrode modified with (a) PhCOOH/Os and (b) SPhCOOH/Os in $NaNO_3$ 0.1 M at 0.1 V s^{-1}.

Table 1 Electrochemical data obtained by cyclic voltammetry in $NaNO_3$ 0.1 M at 0.1 Vs^{-1}

	Au/SPhCOOH/Os	Au/PhCOOH/Os
$E^{o\prime}$/V	0.31	0.30
ΔE_p/V	0.08	0.06
Q/μC cm^{-2}	10.1	10.0
$\Gamma_{Os}/\times 10^{-10}$ mol cm^{-2}	1.04	1.03
FWHM/V	0.17	0.16

agreement with the values obtained from the XPS analysis (see below).

However, for the Au/PhCOOH/Os system it cannot be ruled out the formation of multilayers of the osmium complex since at high overpotentials the electroreduction of 4-carboxybenzenediazonium tetrafluoro-borate may result in radical attack on the free positions of the phenyl rings already attached to the surface leading to multilayer films.[23] However, at low overpotentials formation of monolayer has been demonstrated.[28]

IR Experiment

Polarization Modulated Infrared Reflection Absorption Spec-troscopy (PM-IRRAS) has been employed to confirm the presence and to further characterize the osmium complex on the surface. Fig. 2 compares the spectra of the gold surface before and after the post-functionalization reaction. The infrared peak positions and assignments are summarized in Table 2.

Fig. 2(a) shows the spectra corresponding to the systems Au/PhCOOH and Au/SPhCOOH. In both systems the presence of the carboxylic groups is confirmed by the stretching modes associated with: $\nu_{a\,C=O}$ at 1693 and 1745 cm^{-1}, $\nu_{a\,COO^-}$ at 1540 cm^{-1}. In addition, the bands corresponding to collective ring modes are also observed at $\approx$1600 cm^{-1} ($\nu_{q\,Ph}$, quadrant stretching mode) and $\approx$1400 cm^{-1} ($\nu_{q\,SC}$, semicircular stretching mode). Finally, the band observed at 1365–1329 cm^{-1} can be assigned to the C–H deformation mode (δ_{C-H}). These observations have been reported for the aromatic thiol system by Wells *et al.*[55] The main difference between the PM-IRRAS spectra in Fig. 2(a) is the intensity of the signals and the position of the $\nu_{a\,C=O}$ band for the two sistems. These differences probably arise from the different nature of the gold functionalization. In the case of the thiol derivatized system, the expected result is a monolayer, where there is no appreciable lateral hydrogen bonding between the carboxylic groups of adjacent molecules since the position of the $\nu_{a\,C=O}$ at 1745 cm^{-1} is consistent with this. On the other hand, in the system derived from the diazonium salt electro-reduction, the final result is very dependent on the experiment, even when the reaction is performed under mild conditions.[56] The water content and the total surface coverage and orientation of the deposited molecules would vary among samples, explaining the bigger intensities of the peaks and the shift of

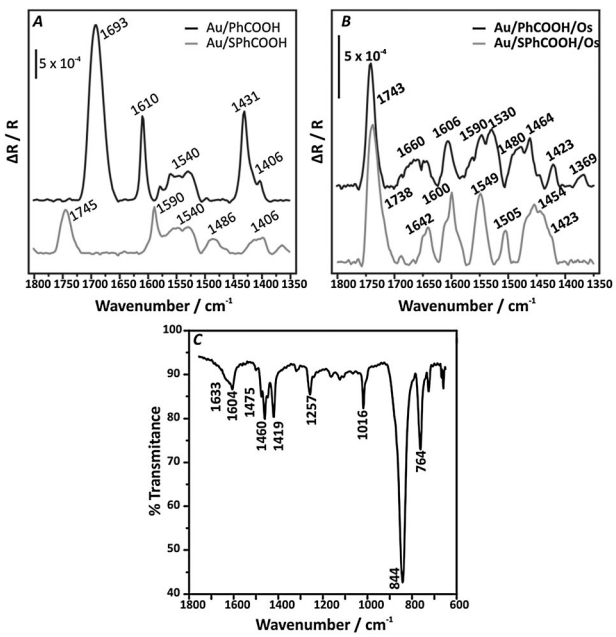

Fig. 2 PM-IRRAS of gold electrodes modified (a) by electro-reduction of 4-carboxybenzenediazonium tetrafluoroborate (black line) and with a monolayer of 4-mercaptobenzoic acid (grey line). (b) PM-IRRAS of the same samples after their post-functionalization with the $[Os(2,2'\text{-bpy})_2ClPyCH_2NH_2]PF_6$ complex. (c) Infrared spectrum of a KBr pellet of the $[Os(2,2'\text{-bpy})_2ClPyCH_2NH_2]PF_6$ complex.

Table 2 PM-IRRAS signal assignment. All frequencies are expressed in cm^{-1}

SPhCOOH	PhCOOH	SPhCOOH/Os	PhCOOH/Os	Os/KBr	
1745	1693	1738	1741		$\nu_{a\,C=O}$
		1642	1660		$\nu_{C=O}$ or amide I
1590	1610	1600	1606	1604	$\nu_{q\,Ph}$
1540	1540	1549	1540		$\nu_{a\,COO^-}$
1486		1505	1480	1475	ν_{Bpy} (or $\nu_{s\,COO}$)
		1454	1464	1460	ν_{Bpy} (or δ_{CH2})
	1431	1423	1423	1419	ν_{Py}
1400	1406				$\nu_{SC\,Ph}$
1365			1369		δ_{C-H}
				1257	δ_{C-H}
				1016	δ_{C-H}
				844	w_{C-H}
				764	w_{C-H}

the $\nu_{a\,C=O}$ band to a lower frequency. This difference is consistent with a hydrogen-bonded dimer structure[55,57] and suggests that the molecules participate in lateral hydrogen bonding.

Fig. 2(b) shows the spectra of the surfaces after the post-functionalization reaction, *i.e.* the spectra corresponding to the systems Au/PhCOOH/Os and Au/SPhCOOH/Os. Basically these spectra show the same bands observed before the post-functionalization plus some new ones. Fig. 2(c) shows the transmission spectrum of a KBr pellet of the $[Os(bpy)_2Cl\ (PyCH_2NH_2)]PF_6$ complex. The band observed at $\approx$1490–1500 cm^{-1} can be attributed to the carboxylate asymmetric stretching mode ($\nu_{a\,COO-}$) or to a bipyridine collective stretching mode (ν_{Bpy}) and the band at $\approx$1423 cm^{-1} can be associated to a pyridine collective mode (ν_{Py}).

Finally, the broad band at 1640–1660 cm^{-1} that is present in both systems and corresponds to the stretching mode of an amide carbonyl ($\nu_{C=O}$ or *amide I*) indicates the covalent bonding of the complex to the surface. The peaks at 1743–1748 cm^{-1} present in both samples and attributed to $\nu_{a\,C=O}$ show that there is still free carboxylic acid after derivatization, which is consistent with the fact that not all of the acid groups form an amide bond with the osmium complex, due to the steric effect resulting from the different areas occupied by each kind of molecule. It is worthy to note, in the case of the samples derived from the diazonium salt electroreduction, the shift of the $\nu_{a\,C=O}$ peak from 1693 cm^{-1} to 1743 cm^{-1} before and after post-funcionalization, respectively.

This fact suggests that during post-functionalization process the hydrogen-bonded dimer structure found in the Au/PhCOOH system is lost. By these results we can follow the derivatization process and confirm that the complex is covalently attached to the surface in both cases.

XPS experiment

In order to gain quantitative chemical information, both systems, Au/PhCOOH/Os and Au/SPhCOOH/Os, were further analyzed by XPS. Fig. 3 shows the spectral regions of interest. In addition to the signals corresponding to the gold substrate, those indicating the presence of carbon, oxygen, nitrogen, chlorine and osmium were also observed. In the second case, S 2p peak was also observed.

Both systems show a doublet centered at 52.5 eV corresponding to the Os 4f level indicating that the osmium center is in its reduced state (Os(II)) (Fig. 3(a)).[58]

Furthermore, the doublet centered at 201 eV indicates the presence of Cl $2p^{27}$ (Fig. 3(b)) which can be assigned to the chloride ligand of the complex. The band at 400.5 eV is associated to the N 1s level (Fig. 3(c)) of the nitrogen atoms of the bipyridine ligand. In the system Au/PhCOOH/Os this peak has also a contribution from the nitrogen in the N=N bonds present in the film formed by the electroreduction of the diazonium salt. This reaction can also produce aryldiazonium radicals which can lead to the formation of *azo* bonds in the deposited film.[56,59]

This way we can confirm that the Os bipyridine complex is on the surface for both systems. Moreover, the S 2p band at 162 eV (Fig. 3(d)), which is characteristic of a thiolate in a Au–S bond[60] can be clearly observed in the Au/SPhCOOH/Os indicating that the 4-mercaptobenzoic acid monolayer does not degrade during the post-functionalization reaction.

Considering the theoretical surface coverage of the Os bipyridine complex mentioned above (1.38×10^{-10} mol cm^{-2}) and that the surface coverage of the thiol molecule in a $\sqrt{3} \times \sqrt{3}$ R30° surface structure is 7.5×10^{-10} mol cm^{-2},[14] then the signal ratio Os : S should be $\approx$1 : 6. From the XPS analysis we obtained a signal ratio Os : S of $\approx$1 : 8, indicating that the efficiency of the post-functionalization reaction was around $\approx$75%. The surface coverage of the osmium complex was obtained from the intensity of the Os 4f signal. In the case of Au/SPhCOOH/Os, a complex surface coverage of 1.2×10^{-10} mol cm^{-2} was obtained. As for the system derived from the diazonium salt reduction, Au/PhCOOH/Os, a similar estimation yielded a surface coverage of 2.6×10^{-10} mol cm^{-2}. These values are consistent with those obtained by the electrochemical analysis.

Finally in the system Au/SPhCOOH/Os the signal ratio Os : N was 1 : 7 which was consistent with the expected value of 1 : 6 confirming that the osmium complex is not degraded during the reaction with carboxylate on the surface. In the case of Au/PhCOOH/Os this ratio was 1 : 11. The higher content of nitrogen in this sample can be associated with the presence of the N=N bonds mentioned above.

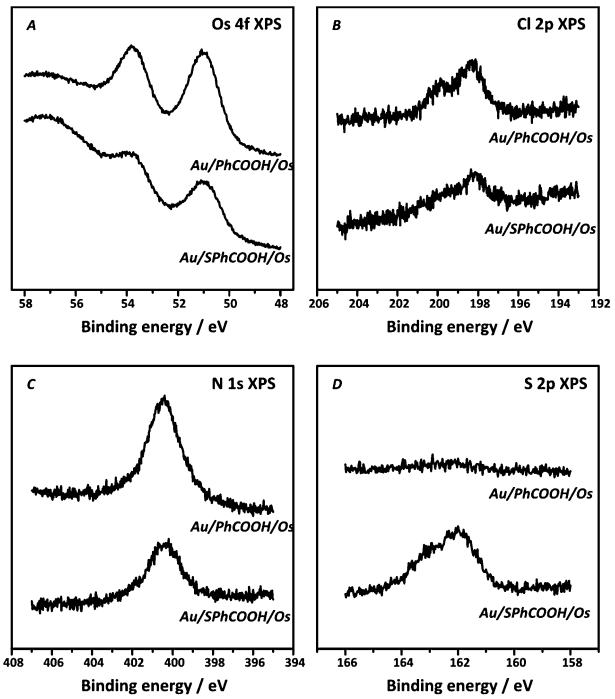

Fig. 3 XPS spectra of Au/PhCOOH/Os and Au/SPhCOOH/Os. For both systems (a) Os 4f, (b) Cl 2p, (c) N 1s and (d) S 2p spectral regions are shown.

Raman experiment

We performed resonant Raman experiments employing a 514.5 nm laser line in order to excite the metal to ligand charge transfer (MLCT) resonance of the Os bipyridine complex.[61]

The observed Raman vibrational features let us confirm that the tethered complex was intact after modification of the surface. In Fig. 4(a) we show the spectra obtained for both systems self-assembled on flat Au and we identify the more intense Os complex signals related to the Os-N stretching (383 cm^{-1}), pyridine bending (670 cm^{-1}) and pyridine stretchings (1022, 1169, 1320, 1482, 1547 and 1606 cm^{-1}) which are in good agreement with previously reported values measured using the same Os complex but attached to a poly-allylamine polymer.[61,62] The presence of the signals associated to the bipyridine groups and the Os–N stretching indicate that the complex was not altered during the surface post-functionalization. On the other hand, not-withstanding the Raman amplification due to the MLCT resonance, the reduced scattering volume leads to a small Raman signal. In order to overcome this problem we have chosen a surface enhanced Raman scattering (SERS) substrate based on Au nanocavity arrays that provide strong enhancements with good homogeneity and reproducibility. These metallic nanocavity arrays, which have been developed by Bartlett and coworkers,[63] have been fabricated *via* an hexagonal close packed self-assembly of polystyrene spheres, followed by an electrochemical Au deposition as described elsewhere.[64,65] In the present study we have used 600 nm diameter Au cavity-arrays (Au cav) with void height $h = 0.4$ which display a 1D-symmetry plasmon at $\sim$520 nm,[66] well tuned to the electronic resonant maximum of the Os bipyridine complex.[61] In Fig. 4(b) we present the Raman spectra on the bipyridine stretching region for samples grown using both surface modification strategies on flat Au (grey lines) and Au nanocavity arrays (black lines). When we use the nanostructured Au substrates we observe no difference in the peak positions but an extra amplification factor of 10 coming from the SERS contribution. This SERS enhancement is not so high because of the plasmonic damping mechanisms present on gold substrates at $\approx$520 nm due to metal electronic interband transition.

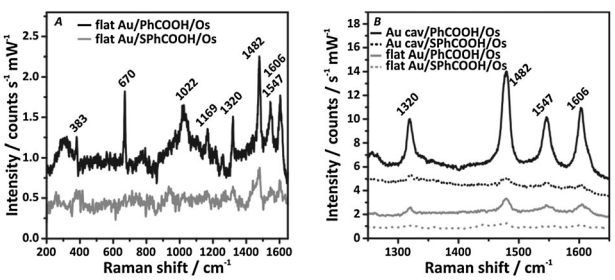

Fig. 4 (a) Resonant Raman spectra of flat gold substrates modified with PhCOOH/Os (black line) and SPhCOOH/Os (grey line). The excitation line was 514.5 nm with a power of 10 mW and the acquisition time was 30 s. The spectra are vertically shifted for clarity of presentation. (b) Comparison of the resonant Raman spectra obtained (bipyridine stretching region) with flat Au (grey lines) and with Au nanocavity substrates (black lines) modified with PhCOOH/Os (full lines) and SPhCOOH/Os (dotted lines). The measurement conditions were 514.5 nm, 10 mW and 30 s for flat Au and 530 nm, 10 mW and 10 s for nanostructured Au.

Using these Au nanocavity substrates spectro-electrochemical experiments were carried out with both Au/PhCOOH/Os and Au/SPhCOOH/Os systems immersed in an electrolyte and under electrochemical control. Fig. 5(a) presents the Raman spectra in the pyridine stretching region for the Au/PhCOOH/Os assembly as a function of the applied potential from 100 mV (reduced Os) to 600 mV (oxidized Os) and back again to 100 mV *vs.* Ag/AgCl reference electrode. We observe that the Raman peaks disappear as the Os bipyridine complex potential moves to oxidation values and they recover intensity

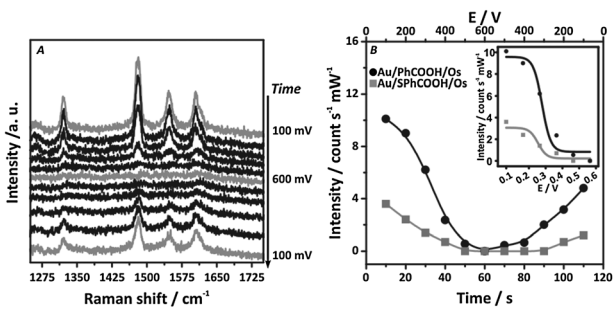

Fig. 5 (a) Raman spectra of Au cav/PhCOOH/Os taken at increasing applied potential: from 0.1 V to 0.6 V and back to 0.1 V. (b) Variation of the intensity of the peak observed at 1483 cm^{-1} for both systems (Au cav/PhCOOH/Os and Au cav/SPhCOOH/Os) as the applied potential is swept. The inset shows the best fit to Nernst equation of this variation.

as the potential goes back to the reduction zone. This can be understood considering that the metal to ligand charge transfer electronic transitions (MLCT) take place at different wavelengths in each case: For Os(II) the transition can be excited with both 514.5 and 530 nm (green) lasers used in the Raman experiment, whereas for the Os(III), it cannot be excited since this MCTL transition corresponds to the ultraviolet region.[61] Therefore, Os(II) is electronic resonant Raman active while Os(III) is not, and therefore the conversion of surface redox sites can be followed by the Raman signals while scanning the electrode potential during the oxidation of the surface Os(II) for several vibrational modes of the osmium complex as presented in Fig. 5(a).

Fig. 5(b) shows the variation of the 1483 cm^{-1} peak intensity as a function of the applied potential for both systems and the inset displays the best fit to the Nernstian response (eqn (1)):

$$I = \frac{P_1}{1 + \exp\left(\frac{RT}{F}(E - P_2)\right)} + P_3 \qquad (1)$$

where P_1, P_2 and P_3 are the fitting parameters. P_2 accounts for the standard potential (E°), whereas P_1 and P_3 account for the arbitrary units of the Raman intensity. In both cases, P_2 turned out to be very close to 0.3 V, which is in perfect agreement with the electrochemical results.

It is apparent that the Raman intensity decreases in the oxidized state (Os(III)) due to the shift of the MLCT transition to the UV with the consequent quenching of the electronic resonance.

The almost complete disappearance of the 1483 cm^{-1} peak respect to the background noise is an indication of good electron coupling of the Os-complex to the Au electrode.[61,67] The peaks re-appear when the sample potential is poised back to values where the original reduced state (Os(II)) prevails, indicating the restoration of the Os Raman resonance. We notice that the signal recovery is not complete, this is caused by a photo-electrochemical mechanism already observed and discussed elsewhere.[61] From this analysis we conclude that both Au–C and Au–S types of bond yield systems with similar electrochemical response and molecule-to-substrate connec-tivity.

STM experiment

Typical STM images of the system Au(111)/PhCOOH/Os show the Au(111) terraces covered by a dense net of randomly distributed bright spots that completely masks the underlying substrate features. In Fig. 6(b) (left) an STM image (V_{bias} = 1.5 V, $I_{setpoint}$ = 0.35 nA) is shown after shaving lithography, *i.e.*, repetitively scanning the STM tip on a square region at 3 nA and 1 V, followed by an increase in the scan size in order to observe the window opened at the center of the image. The height difference, measured by a cross-section (Fig. 6(a), right), between the covered and the uncovered (bare Au(111)) regions was 1.2 ± 0.3 nm. The theoretical structure, obtained by DFT calculations mentioned above, yielded an estimated height for the osmium complex plus benzoic acid monolayer (measured from the Os atom to the Au surface) of 1.4 nm. Although height measurement from STM images should be taken with care due to the convolution of topographic and electronic information, the height value measured by STM was in the order of that calculated by DFT, which would indicate that no multilayers of the osmium complex were formed, as also revealed by XPS. STM images do not show any clear dependence with the bias voltage.

Less covered regions were also imaged, as in Fig. 6(b), left. From the analysis of several cross sections of the image we can conclude that the height of the spots is 0.80 ± 0.15 nm (Fig. 6(b), right). This would correspond to the height of the osmium complex only (the background is completely covered by the benzoic acid layer), in accordance with the estimated theoretical height of the osmium complex (0.8 nm). An estimation of the average size of the spots was also made by performing the power spectral density analysis (PSD) provided by the microscope software (after high-pass filtering of the image), yielding an average aggregate size of ≈4.35 nm (data not shown) which is much higher than the expected for a single complex molecule and could be attributed to several factors: a tip–sample convolution artifact, some complex aggregation, or to the incomplete removal of excess reactives or by- products following post-functionalization. The latter would account for the Os/N ratio obtained by XPS.

Similar results were observed for the osmium complex covalently attached to a 4-mercaptobenzoic acid SAM (Fig. 7). Also in this case, a dense net of poorly defined bright spots can be observed (Fig. 7(a), left). Again, after opening a window in the layer by scanning the STM tip at 3 nA and 1 V, a layer thickness of 1.0 ± 0.2 nm was observed (Fig. 7(a) left; V_{bias} = 1.5 V, $I_{setpoint}$ = 0.35 nA). The height (0.8 ± 0.2 nm) and the average size of the spots from PSD (≈4 nm) are similar to those observed for the Au/PhCOOH/Os system.

STM images of benzoic acid and 4-mercaptobenzoic acid layers on Au(111) do not show the features that are observed following the post-functionalization process of the SAMs with the Os complex.

Projected density of states obtained with density functional theory

Periodic boundary density functional calculations were conducted on model systems representing benzene (Ph) and mercaptobenzene (SPh) adsorbed on Au(111), *i.e.*, Au(111)/SPh and Au(111)/Ph. The relaxed structures, depicted in Fig. 8, correspond to bridge and top binding for the S–Au and C–Au links, respectively. Total and projected density of states (PDOS) were computed for these systems. A very interesting result was found concerning the projections of the p orbitals of the C and the S atoms, shown in Fig. 9.

The delocalization of the PDOS for a given atomic orbital across the energy spectrum is indicative of a strong involvement in the electronic structure of the extended system. This is seen for the p orbitals of the sulfur atom attached to gold in Au(111)/SPh. In contrast, the features of the p orbitals of the link carbon atom in Au(111)/Ph are sharp and show little delocalization.

Fig. 9 displays also the PDOS corresponding to the non-interacting systems (grey line), with the adsorbates placed approximately 4 Å above the substrate.

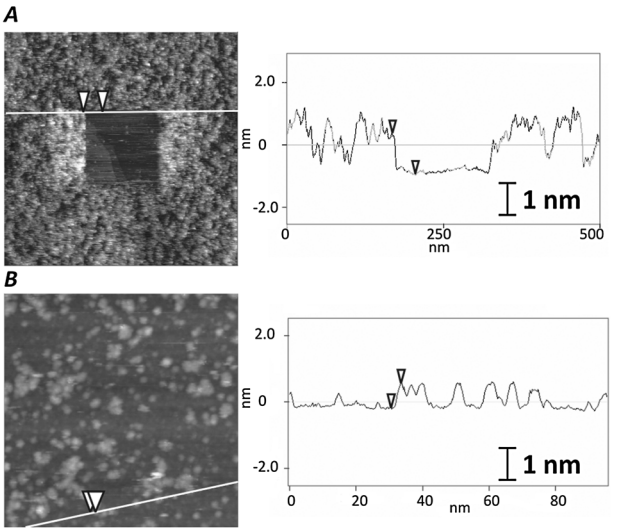

Fig. 6 (a – Left) 500 × 500 nm^2 in air STM image of a Au (111) sample derivatized with benzoic acid and post-functionalized with $[Os(2,2'\text{-bpy})_2Cl(py\text{-}CH_2\text{-}NH_2)]^+$, taken at 350 pA and 1.5 V after shaving lithography. (Right) Cross section of the image showing the height of the layer. (b – Left) 100 × 100 nm^2 in air STM image taken at 500 pA and 1.3 V showing lower spot density. Individual spots can be seen. (Right) Cross section of the image showing the height of the features.

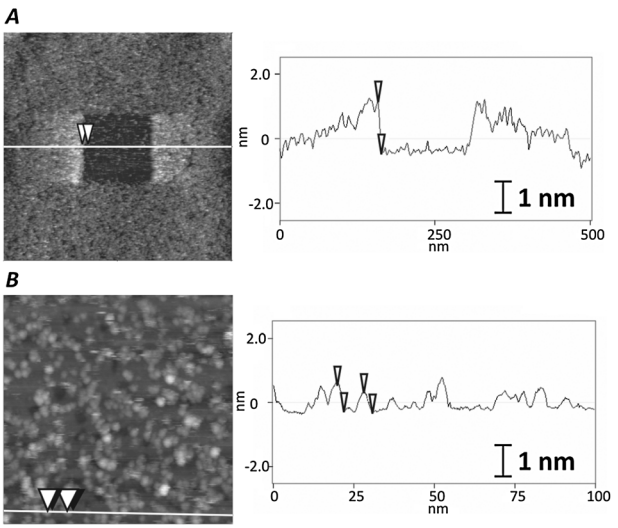

Fig. 7 (a – Left) 500 × 500 nm^2 in air STM image of a Au (111) sample derivatized with 4-mercaptobenzoic acid and post-functionalized with $[Os(2,2'\text{-bpy})_2Cl(py\text{-}CH_2\text{-}NH_2)]^+$, taken at 350 pA and 1.5 V after shaving lithography. (Right) Cross section of the image showing the height of the layer. (b – Left) 100 × 100 nm^2 in air STM image taken at 500 pA and 1.3 V showing lower spot density. Individual spots can be seen. (Right) Cross section of the image showing the height of the features.

In this situation the electronic structures of the molecule and the slab are decoupled. Comparison of the different curves shows that the adsorption of mercaptobenzene induces a strong hybridization of the sulfur p orbitals, which experience a substantial mixing with the metallic states, spanning a broad region around the Fermi level.

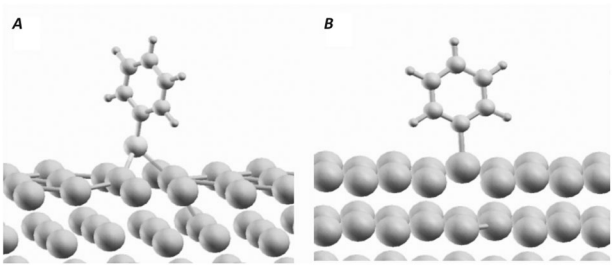

Fig. 8 DFT optimized structures for (a) Au (111)/SPh and (b) Au (111)/Ph. The relaxed geometries for the S–Au and the C–Au bonds correspond to bridge and top configurations, respectively.

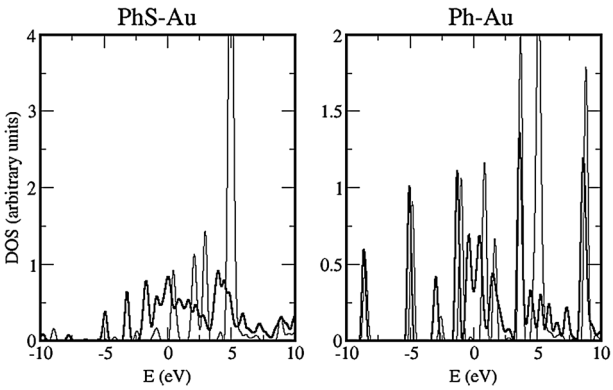

Fig. 9 Projected Density of States (PDOS) for the p orbitals of the S and the C atoms bonded to gold. For comparison, the grey curves depict the PDOS corresponding to the isolated molecules, prior to adsorption. A larger electronic delocalization is observed for the SPh molecule (left panel). Fermi levels are 5.34 eV for Au/(111)/SPh and 5.17 eV for Au(111)/Ph.

On the other hand, the pattern of the p orbitals of the C atom is only moderately affected upon binding. These results clearly suggest that the electronic coupling between the molecule and the surface must be more important for mercaptobenzene than for benzene. It is worth noting that no delocalization was observed in the PDOS of the other orbitals of both systems.

Conclusions

In the present article we report the modification of gold electrodes with a bipyridine Os complex tethered to the surface by two alternative bonds: Au–C and by Au–S. A variety of complemmentary spectroscopic and microscopic techniques have confirmed the covalent bond of the molecularly intact complex to the underlying Au surface.

The post-functionalization *via* an amide bond of the osmium complex to the benzoic acid tethered to the surface has been confirmed by vibrational and electron spectroscopies. The surface coverage of the redox molecule has been determined to correspond to a monolayer from the integrated redox charge in cyclic voltammetry, XPS and STM. Furthermore, STM line profiles confirmed the expected molecular heights for the benzoic acid and the redox complex.

A DFT study of the aromatic linker of the Os complex has shown the calculated molecular geometry at the surface in

good agreement with the STM profiles, and differences in the electron coupling. However, tunneling spectroscopic studies of these two Au–S and Au–C constructs in the STM "tunneling" gap configuration could not detect these differences in a tow-step ET between the molecule and the contacts (tip and substrate) with partial vibrational relaxation.[68]

Acknowledgements

ANCyPT, PICT 1146, Red Nano-tecnología PAE-2004 No. 22711, Centro Interdisciplinario de Nanociencia y Nano-tecnologia (CINN) PAE-2006 No. 37063.

References

1 G. Valincius, G. Niaura, B. Kazakeviciene, Z. Talaikyte, M. Kazemekaite, E. Butkus and V. Razumas, *Langmuir*, 2004, **20**, 6631.
2 S. Tsujimura, M. Fujita, H. Tatsumi, K. Kano and T. Ikeda, *Phys. Chem. Chem. Phys.*, 2001, **3**, 1331.
3 I. Willner and B. Willner, *Pure Appl. Chem.*, 2002, **74**, 1773.
4 N. A. Anderson, X. Ai, D. T. Chen, D. L. Mohler and T. Q. Lian, *J. Phys. Chem. B*, 2003, **107**, 14231.
5 *Introducing Molecular Electronics*, Springer, Berlin Heidelberg, 2005.
6 W. Haiss, T. Albrecht, H. Van Zalinge, S. J. Higgins, D. Bethell, H. Höbenreich, D. J. Schiffrin, R. J. Nichols, A. M. Kuznetsov, J. Zhang, Q. Chi and J. Ulstrup, *J. Phys. Chem. B*, 2007, **111**, 6703–6712.
7 H. O. Finklea and D. D. Hanshew, *J. Am. Chem. Soc.*, 1992, **114**, 3173–3181.
8 R. J. Forster, *Inorg. Chem.*, 1996, **35**, 3394.
9 R. J. F. Forster and L. R. Faulkner, *J. Am. Chem. Soc.*, 1994, **116**, 5453.
10 D. Acevedo and H. D. Abruña, *J. Phys. Chem.*, 1991, **95**, 9590–9594.
11 J. F. Smalley, S. B. Sachs, C. E. D. Chidsey, S. P. Dudek, H. D. Sikes, S. E. Creager, C. J. Yu, S. W. Feldberg and M. D. Newton, *J. Am. Chem. Soc.*, 2004, **126**, 14620–14630.
12 J. F. Smalley, H. O. Finklea, C. E. D. Chidsey, M. R. Linford, S. E. Creager, J. P. Ferraris, K. Chalfant, T. Zawodzinsk, S. W. Feldberg and M. D. Newton, *J. Am. Chem. Soc.*, 2003, **125**, 2004–2013.
13 C. Vericat, M. E. Vela, G. Benitez, P. Carro and R. C. Salvarezza, *Chem. Soc. Rev.*, 2010, **39**, 1805–1834.
14 J. C. Love, L. A. Estroff, J. K. Kriebel, R. G. Nuzzo and G. M. Whitesides, *Chem. Rev.*, 2005, **105**, 1103–1107.
15 M. Delamar, R. Hitmi, J. Pinson and J. M. Saveant, *J. Am. Chem. Soc.*, 1992, **114**, 5883–5884.
16 C. Bourdillon, M. Delamar, C. Demaille, R. Hitmi, J. Miroux and J. Pinson, *J. Electroanal. Chem.*, 1992, **336**, 113.
17 Y. C. Liu and R. L. McCreery, *J. Am. Chem. Soc.*, 1995, **117**, 11254–11259.
18 Y. C. Liu and R. L. McCreery, *Anal. Chem.*, 1997, **69**, 2091.
19 F. Anariba, S. H. DuVall and R. L. McCreery, *Anal. Chem.*, 2003, **75**, 3837–3844.
20 A. J. Downard, *Langmuir*, 2000, **16**, 9680.
21 A. J. Downard, *Electroanalysis*, 2000, **12**, 1085.
22 B. Ortiz, C. Saby, G. Y. Champagne and D. Bélanger, *J. Electroanal. Chem.*, 1998, **455**, 75–81.
23 J. K. Kariuki and M. T. McDermott, *Langmuir*, 1999, **15**, 6534–6540.
24 P. Allongue, M. Delamar, B. Desbat, O. Fagebaume, R. Hitmi, J. Pinson and J.-M. Saveant, *J. Am. Chem. Soc.*, 1997, **119**, 201–207.
25 C. H. Villeneuve, J. Pinson, M.-C. Bernard and P. Allongue, *J. Phys. Chem. B*, 1997, **101**, 2415–2420.
26 M. P. Stewart, F. Maya, D. V. Konsynkin, S. M. Dirk, J. J. Stapelton, C. L. McGuiness, D. L. Allara and J. M. Tour, *J. Am. Chem. Soc.*, 2004, **126**, 370–378.
27 A. Laforgue, T. Addou and D. Belanger, *Langmuir*, 2005, **21**, 6855.
28 A. M. Ricci, C. Bonazzola and E. J. Calvo, *Phys. Chem. Chem. Phys.*, 2006, **8**, 4297.
29 A. Adenier, M.-C. Bernard, M. M. Chehimi, E. Cabet-Deliry, B. Desbat, O. Fagebaume, J. Pinson and F. Podvorica, *J. Am. Chem. Soc.*, 2001, **123**, 4541.
30 M.-C. Bernard, A. Chausse′, E. Cabet-Deliry, M. M. Chehimi, J. Pinson, F. Podvorica and C. Vautrin-Ul, *Chem. Mater.*, 2003, **15**, 3450–3461.
31 B. L. Hurley and R. L. McCreery, *J. Electrochem. Soc.*, 2004, **151**, B252–B259.
32 F. Anariba, U. Viswanathan, D. F. Bocian and R. L. McCreery, *Anal. Chem.*, 2006, **78**, 3104–3112.
33 J. Lyskawa and D. Bélanger, *Chem. Mater.*, 2006, **18**, 4755–4763.
34 D. Evrard, F. Lambert, C. Policar, V. Balland and B. Limoges, *Chem.–Eur. J.*, 2008, **14**, 9286–9291.
35 S. Boland, F. Barriere and D. Leech, *Langmuir*, 2008, **24**, 6351–6358.
36 A.-E. Radi, V. Lates and J.-L. Marty, *Electroanalysis*, 2008, **20**, 2557–2562.
37 S. Griveau, D. Mercier, C. Vautrin-Ul and A. Chaussé, *Electrochem. Commun.*, 2007, **9**, 2768–2773.
38 S. Liu, L. Wang and F. Zhao, *J. Electroanal. Chem.*, 2007, **602**, 55–60.
39 G. Liu, J. Liu, T. Bocking, P. K. Eggers and J. J. Gooding, *Chem. Phys.*, 2005, **319**, 136–146.
40 V. Vijaikanth, J.-F. Capon, F. Gloaguen, P. Schollhammer and J. Talarmin, *Electrochem. Commun.*, 2005, **7**, 427–430.
41 N. G. Tognalli, A. Fainstein, C. Vericat, M. E. Vela and R. C. Salvarezza, *J. Phys. Chem. B*, 2006, **110**, 354–360.
42 M. A. D. Millone, M. E. Vela, R. C. Salvarezza, T. B. Creczinsky-Pasa, N. G. Tognalli and A. Fainstein, *ChemPhysChem*, 2009, **10**, 1927–1933.
43 A. M. Ricci, C. Rolli, S. Rothacher, L. Baraldo, C. Bonazzola, E. J. Calvo, N. Tognalli and A. Fainstein, *J. Solid State Electrochem.*, 2007, **11**, 1511–1520.
44 M. Breiter, C. A. Knorr and W. Volkl, *Z. Elektrochem.*, 1955, **64**, 681.
45 D. A. J. Rand and R. Woods, *J. Electroanal. Chem.*, 1972, **35**, 209–218.
46 B. J. Barner, M. J. Green, E. I. Saez and R. M. Corn, *Anal. Chem.*, 1991, **63**, 55–60.
47 M. J. Green, B. J. Barner and R. M. Corn, *Rev. Sci. Instrum.*, 1991, **62**, 1426–1430.
48 B. L. Frey, R. M. Corn and S. C. Weibel, *Polarization Modulation Approaches to Reflection-Absorption Spectroscopy. In Handbook of Vibrational Spectroscopy*, John Wiley & Sons, 2001.
49 P. Giannozzi, *J. Phys.: Condens. Matter*, 2009, **21**, 395502.
50 D. Vanderbilt, *Phys. Rev. B: Condens. Matter*, 1990, **41**, 7892.
51 J. P. Perdew, K. Burke and M. Ernzerhof, *Phys. Rev. Lett.*, 1996, **77**, 3865.
52 H. Monkhorst and J. Pack, *Phys. Rev. B: Solid State*, 1976, **13**, 5188.
53 A. J. Bard and L. R. Faulkner, *Electrochemical Methods*, John Wiley and Sons, New York, 2001.
54 C. Danilowicz, E. Corton and F. Battaglini, *J. Electroanal. Chem.*, 1998, **445**, 89.
55 M. Wells, D. L. Dermody, H. C. Yang, T. Kim and R. M. Crooks, *Langmuir*, 1996, **12**, 1989–1996.
56 A. M. Ricci, L. P. M. D. Leo, F. J. Williams and E. J. Calvo, *Paper in process*, 2010.
57 R. G. Nuzzo, L. H. Dubois and D. L. Allara, *J. Am. Chem. Soc.*, 1990, **112**, 558–559.
58 D. Eliche-Quesada, J. M. Mérida-Robles, E. Rodríguez-Castellón and A. Jiménez-López, *Appl. Catal., A*, 2005, **279**, 209–221.
59 P. Doppelt, G. Hallais, J. Pinson, F. Podvorica and S. Verneyre, *Chem. Mater.*, 2007, **19**, 4570–4575.
60 C. Vericat, M. E. Vela, G. Andreasen and R. C. Salvarezza, *Langmuir*, 2001, **17**, 4919–4924.
61 N. Tognalli, A. Fainstein, C. Bonazzola and E. J. Calvo, *J. Chem. Phys.*, 2004, **120**, 1905.
62 N. G. Tognalli, A. Fainstein, E. Calvo, C. Bonazzola, L. Pietrasanta, M. Campoy-Quiles and P. Etchegoin, *J. Chem. Phys.*, 2005, **123**, 044707–044701/044709.

63 P. N. Bartlett, P. R. Birkin and M. A. Ghanem, *Chem. Commun.*, 2000, 1671.
64 N. Tognalli, P. Scodeller, V. Flexer, R. Szamocki, A. Ricci, M. Tagliazucchi, E. J. Calvo and A. Fainstein, *Phys. Chem. Chem. Phys.*, 2009, **11**, 7412–7423.
65 P. Allongue, C. H. d. Villeneuve, G. Cherouvrier, R. Cortés and M.-C. Bernard, *J. Electroanal. Chem.*, 2003, **550–551**, 161–174.
66 P. D. Lacharmoise, N. G. Tognalli, A. R. Goñi, M. I. Alonso, A. Fainstein, R. M. Cole, J. J. Baumberg, J. G. d. Abajo and P. N. Bartlett, *Phys. Rev. B: Condens. Matter Mater. Phys.*, 2008, **78**, 125410.
67 P. Scodeller, V. Flexer, R. Szamocki, E. J. Calvo, N. Tognalli, H. Troiani and A. Fainstein, *J. Am. Chem. Soc.*, 2008, **130**, 12690–12697.
68 A. M. Ricci, E. J. Calvo, S. Martin and R. J. Nichols, *J. Am. Chem. Soc.*, 2010, **132**, 2494–2495.

